Characteristics of the Optic Nerve Head in Myopic Eyes Using Swept-Source Optical Coherence Tomography

Dan Cheng,[1] Kaiming Ruan,[1] Minhui Wu,[1] Yilin Qiao,[1] Weiqian Gao,[1] Hengli Lian,[1] Meixiao Shen,[1] Fangjun Bao,[1] Yizeng Yang,[1] Jun Zhu,[1] Haiying Huang,[1] Xianwei Meng,[1] Lijun Shen,[1,2] and Yufeng Ye[1]

[1]The Affiliated Eye Hospital of Wenzhou Medical University, Hangzhou, Zhejiang, China
[2]Department of Ophthalmology, Zhejiang Provincial People's Hospital, Hanghzou, Zhejiang, China

Correspondence: Lijun Shen, The Affiliated Eye Hospital of Wenzhou Medical University, 618 Fengqi East Road, Hangzhou, Zhejiang 310000, China;
ljshenysg@163.com.
Yufeng Ye, The Affiliated Eye Hospital of Wenzhou Medical University, 618 Fengqi East Road, Hangzhou, Zhejiang 310000, China;
yyf0571@mail.eye.ac.cn.

LS and YY contributed equally to this research.

Received: March 24, 2022
Accepted: May 25, 2022
Published: June 22, 2022

Citation: Cheng D, Ruan K, Wu M, et al. Characteristics of the optic nerve head in myopic eyes using swept-source optical coherence tomography. *Invest Ophthalmol Vis Sci.* 2022;63(6):20.
https://doi.org/10.1167/iovs.63.6.20

Purpose. To investigate the characteristics of the optic nerve head (ONH) in myopia using swept-source optical coherence tomography (SS-OCT).

Methods. Participants were divided into three groups according to the axial length (AL). The optic disc morphology, retinal nerve fiber layer (RNFL) thickness, and radial peripapillary capillary (RPC) vessel density (VD), optic disc tilt, rotation, Bruch's membrane opening distance (BMOD), border length (BL), border tissue angle, focal lamina cribrosa (LC) defects, β- and γ-zone peripapillary atrophy (PPA), microvasculature dropout (MvD), choroidal thickness (CT), and the choroidal vascularity index (CVI) were compared. Linear regression analysis evaluated relationships between spherical equivalent, AL, and ONH parameters.

Results. One hundred five, 98, and 118 eyes were included in groups 1, 2, and 3, respectively. With AL increasing, the mean, superior and temporal CT, central mean and temporal, pericentral mean, inferior and nasal RPC VD, and temporal CVI decreased, whereas the mean and temporal RNFL thickness, optic disc, RIM and β-PPA area, presence and area of γ-PPA, BMOD and BL increased. Compared to other groups, group 3 depicted a larger cup area, more focal LC defect and total and juxtapapillary MvD; a lower central superior, inferior and nasal, pericentral superior, and temporal RPC VD. Group 1 demonstrated more tilted disc, larger inferior and nasal CT, mean, superior, inferior, and nasal CVI.

Conclusions. Myopia eyes have larger ONH changes, PPAs, regional RNFL, and MvD, but smaller regional CTs, RPC VD, and CVIs. SS-OCT may be useful in detecting ONH variations during myopia.

Keywords: myopia, optic nerve head, peripapillary, OCT, OCTA

Myopia is the most common eye disease worldwide, leading to irreversible vision loss and blindness,[1] with its prevalence increasing to 90% among teenagers and young adults, particularly in Asia.[2,3] Axial myopic eyes have a multitude of histological changes in the posterior hemisphere of the globe, most notably at the posterior pole and optic nerve head (ONH).[4,5] In recent years, myopic optic discs have attracted significant interest.[6–9] Moreover, with posterior scleral remodeling, myopic eyes present characteristic ONH changes, including optic disc tilt, rotation, parapapillary atrophy, lamina cribrosa (LC) defects, and microvasculature dropout (MvD). These ONH deformations are often associated with vision loss, visual field defects, disruption of parapapillary microvasculature, or mechanical dysfunction of the laminar beams.[8,10,11] Understanding the ONH features in myopic eyes is of great importance in investigating the development of myopic optic disc, mechanism of axial myopia and related peripapillary changes and atrophies, along with early detection of glaucoma, retinoschisis, and other complications.

Swept-source optical coherence tomography (SS-OCT) was originally described in 1995 and has recently matured for use in retinal imaging.[12,13] With the incorporation of longer wavelengths than those recorded with conventional spectral domain (SD) devices, SS-OCT enables retinal imaging with an increasing depth of resolution and can simultaneously provide imaging of the vitreous, retina and choroid, as well as microvasculature with OCT angiography (OCTA).[14,15]

Knowledge concerning the characteristics of myopic optic discs using SS-OCT is limited. Previous studies focused on a few features of myopic ONH based on small samples or SD-OCTs.[9,11,16,17] However, despite the high cost, the advantages of techniques would provide more accurate tissue profile. In addition, the information on peripapillary choroidal perfusion in myopic eyes is unclear. The current study aimed to characterize the structural and microvasculature changes in the ONH in healthy myopia and evaluate their association with spherical equivalent (SE) and axial length (AL) using SS-OCT and SS-OCTA.

Methods

Participants

The study protocol adhered to the tenets of the Declaration of Helsinki and was approved by the ethics committee of Wenzhou Medical University (2019-078-K-77). All participants were informed about the content, and informed consent was obtained. Healthy individuals were recruited prospectively from September to December 2021 at the Affiliated Eye Hospital of Wenzhou Medical University in Hangzhou.

We divided the study participants into three groups: group 1 (AL $\leq$ 25 mm), group 2 (25 $>$ AL $<$ 26 mm), and group 3 (AL $\geq$ 26 mm). Each participant underwent a complete ocular examination, which included best-corrected visual acuity, autorefractometry, and keratometry using an autorefractor (AR-1, Nidek, Hiroishi, Japan), AL using an optical biometer (IOL Master 700; Carl Zeiss Meditec, Jena, Germany), central corneal thickness (CCT, Pentacam HR type 70900), slit-lamp examination, intraocular pressure (IOP) using Goldmann applanation tonometry, anterior chamber angle examination by gonioscopy, fundoscopy, visual field testing, and SS-OCT/OCTA examinations (VG200S; SVision Imaging, Henan, China).

The inclusion criteria were as follows: healthy individuals aged between 18 and 40 years, best-corrected visual acuity of 20/25 or better, astigmatism within $\pm$ 2.0 D and less than 2.0 D difference in the refractive error between the two eyes, and IOP $<$ 21 mm Hg. The exclusion criteria were visual field defects; glaucomatous ONHs[18–20]; various pathologic changes on the myopic fundus or OCT, such as staphyloma, lacquer cracks, myopic macular degeneration; and history of vitreoretinal disease, opaque media, intraocular surgery, or a systemic disease such as diabetic retinopathy and hypertension. The right eye of each participant was selected.

SS-OCT and OCTA Image Acquisition

The SS-OCT/OCTA system (VG200S; SVision Imaging, Henan, China) contained an SS laser with a central wavelength of approximately 1050 nm and scan rate of 200,000 A-scans per second. Measurements were conducted from 13:30 to 17:00 to minimize the potential impact of diurnal variation.[21] A cutoff signal-strength index value $\geq$6 was used as the inclusion criterion. Structural OCT centered on the fovea was performed using 18 radial scan lines, each of which was 12 mm long. The ONH angiography imaging was performed using 4.5 $\times$ 4.5 mm scans.

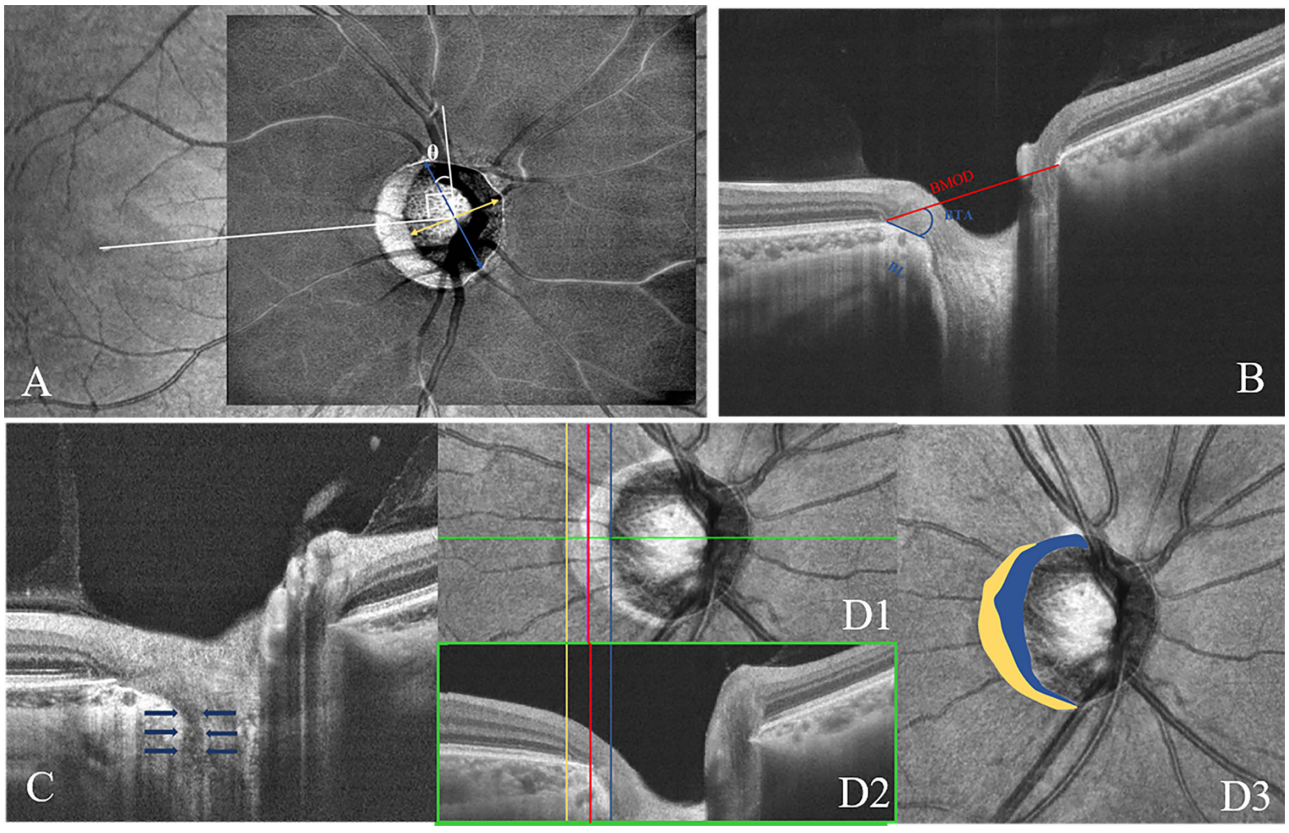

Figure 1. ONH and peripapillary structural parameter measurement. **(A)** Measurement of the optic disc tilt ratio and rotation degree by infrared fundus photography on OCT. The optic disc tilt was evaluated as the ratio between the longest and shortest diameters of the optic disc. The rotation was defined as the deviation of the long axis of the optic disc from the reference line (θ), which is 90° from a horizontal line connecting the fovea and the center of the optic disc. **(B)** ONH parameter measurement in the B-scan image. The BMO distance was evaluated between both sides of BMO. The BL was measured as the straight-line distance between the BMO point and the BT and scleral end. The BT angle (BTA) was defined as the angle between the BMO reference plane and the BT. **(C)** B-scan OCT image demonstrating focal LC defect (*blue arrows*). **(D)** Determination of the presence and area of β-zone and γ-zone PPA. The *yellow*, *red*, and *blue lines* present the boundaries of the RPE, Bruch's membrane, and optic disc margin, respectively **(D1, D2)**. The β-zone PPA is marked in *yellow* and the γ-zone PPA is marked in *blue* **(D3)**.

Investigative Ophthalmology & Visual Science

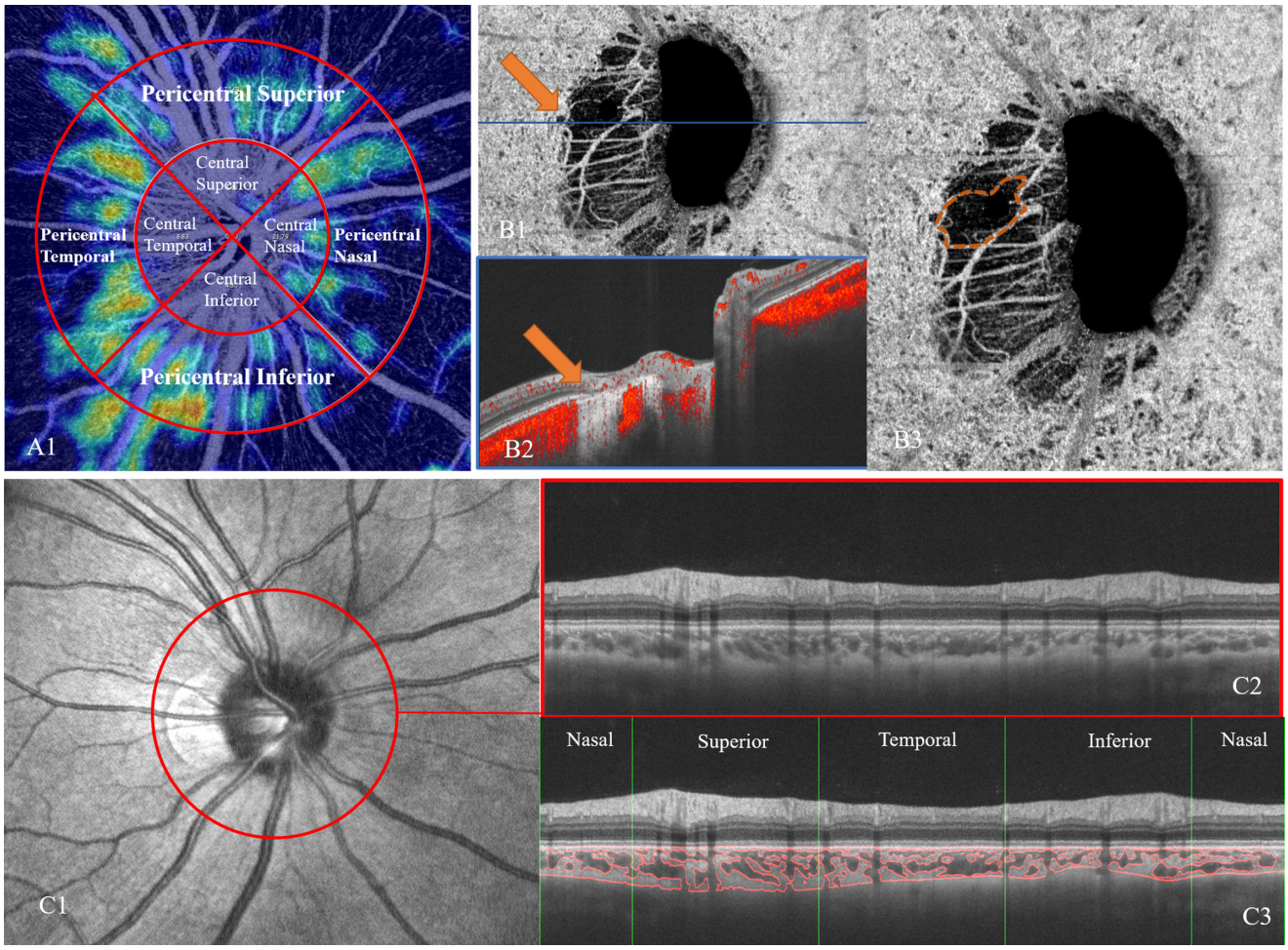

Figure 2. Measurement of ONH and peripapillary microvasculature parameters. **(A)** The radial peripapillary capillary was divided into central and pericentral regions to analyze the vessel density with diameters of 2 and 4 mm, respectively. **(B1)** Determination of the presence of the MvD within the PPA deep retinal layer on the choroidal vessel density map of ONH OCTA images. MvD was well demarcated on the enlarged **(B3)** en-face choroidal vessel density map (*orange dotted outline*) and confirmed on the B-scan OCTA image **(B2)**. **(C)** The CVI was measured along the outer edge of a 3.4-mm-diameter circle centered on the ONH in the glaucoma analysis mode (**C1, C2**) using a custom-built imaging software in MATLAB. The CVI was calculated into four parts, including superior, inferior, nasal, and temporal **(C3)**.

In the glaucoma analysis mode, the mean and vertical cup-to-disc ratio, area of the optic disc, cup and rim, and cup volume were assessed. The peripapillary retinal nerve fiber layer (RNFL) thickness was divided into four sectors: superior (S), temporal (T), inferior (I), and nasal (N). Radial peripapillary capillary (RPC) vessel density (VD) was divided into eight sectors (Fig. 2A): central superior, central temporal, central inferior, central nasal, pericentral superior, pericentral temporal, pericentral inferior, and pericentral nasal. The central region was defined as a 2-mm-diameter circle centered on the ONH. The pericentral region extends from the edge of the central region and has an outer diameter of 4 mm with ONH at the center (Fig. 2A1).

Measurement of ONH and Peripapillary Structural Parameters

Using the embedded tools, the optic disc tilt[11] was evaluated as the ratio between the longest and shortest diameters of the optic disc on the en-face image (Fig. 1A). Optic discs were classified as tilted when the tilt ratios exceeded 1.30. Optic disc rotation was defined as the deviation of the long axis of the optic disc from the reference line (θ), which was 90° from the horizontal line connecting the fovea and the center of the optic disc. From the long axis of the optic disc to the reference line, a positive value indicated clockwise rotation and a negative value indicated counterclockwise rotation in the right eye. The optic disc was classified as having significant rotation when the degree of rotation exceeded 15°. On the horizontal B-scan across the midpoint of the longest axis of the disc, the distance between both sides of the Bruch's membrane opening (BMO) points was defined as the BMO[9] distance (BMOD, Fig. 1B). The border length (BL) was measured as the straight-line distance between the temporal BMO point and the border tissue (BT) and scleral end. The BT angle was defined as the angle between the BMO reference plane and BT. A focal LC defect was defined as an anterior laminar surface irregularity violating the normal smooth curvilinear contour with a maximal diameter greater than 100 µm and a depth greater than 30 µm, which should be present in two neighboring line scans (Fig. 1C).[22]

Investigative Ophthalmology & Visual Science

In the peripapillary region, with the B-scan images (Fig. 1.D1), we drew three demarcation boundaries on the en-face view of the infrared image: the retinal pigment epithelium opening (RPEO, which is the area without the RPE), BMO, and clinical disc margin. The areas between RPEO and BMO as well as BMO and clinical disc margin were defined as β-zone and γ-zone peripapillary atrophy (PPA), respectively (Fig. 1D). The β- PPA was defined as the area where RPE was absent, but BM was present, and γ-PPA was defined as the area where both BM and RPE were not present.

Measurement of ONH and Peripapillary Microvasculature Parameters

The MvD was defined as a complete loss of microvasculature on the choroidal layer OCTA en-face images within the PPA (Fig. 2B). Parapapillary MvD was classified as non-juxtapapillary and juxtapapillary MvD, located in the β-zone and γ-zone, respectively.[7] Using a custom-built imaging software implemented in MATLAB R2017a (Mathworks, Natick, MA, USA),[23,24] the choroidal thickness (CT) and the choroidal vascularity index (CVI) were measured in B-scan images along the outer edge of a 3.4-mm-diameter circle centered on the ONH in the glaucoma analysis pattern (Fig. 2C). After semiautomatic segmentation, the segmentations of the RPE-Bruch's membrane complex and choroid-sclera interface were adjusted manually. Each image was binarized to demarcate the luminal area (LA) and stromal area (SA). Additionally, the mean CT, total choroidal area, LA, and SA were calculated. The CVI was defined as the ratio of LA to total choroidal area. CT and CVI were calculated in the total peripapillary area and four parts, including the superior, inferior, nasal, and temporal regions.

Two independent observers (MW and WG) identified the ONH and peripapillary parameters. Disagreements between the observers were resolved by a third adjudicator (YQ).

Statistical Analysis

R version 4.1.1. was used. Interobserver agreement was assessed using the Bland-Altman and kappa (κ) analyses. The limits of agreement were defined as the mean differences of the two measurements $\pm$ 1.96 standard deviation of the difference. Groups were compared using the χ^2 test, analysis of variance test, or Wilcoxon test, whichever was appropriate. Univariate and multivariate linear regression analyses were used to identify the ONH and peripapillary variables with a statistically significant contribution to SE and AL. The relationships between SE, AL and mean RNFL thickness, CT, RPC VD, and CVI were evaluated using univariate linear regression. Multivariate linear regression analyses were used to determine the association between SE, AL and regional RNFL thickness, CT, RPC VD, and CVI. Parameters with P values < 0.05 in the univariate analysis were included in the multivariate models. Statistical significance was set at $P < 0.05$.

Results

Demographic Data

A total of 321 eyes of 321 individuals with AL ranging from 22.55 mm to 31.28 mm (mean: 25.65 $\pm$ 1.35 mm) and SEs ranging from + 0.50 D to −15.63 D (mean: −5.11 $\pm$ 2.64 D) were included (Table 1). Bland-Altman plots presenting the interobserver agreement revealed no systemic differences (Fig. 3). The repeatability (κ) of the presence of focal LC defects and MvD, direction of the optic disc rotation, and type of MvD were 0.928, 0.730, 0.894, and 0.925, respectively. The mean age was 28.43 $\pm$ 6.25 years. Of all, 109 were men and 212 were women. As there were significant differences in the sex distribution in groups 1 and 3, we randomly selected 50 (25 men and 25 women) and 96 (48 men and 48 women) participants from groups 1 and 3, respectively. The results showed no differences between the ONH parameters between men and women. There were no significant differences in IOP or CCT among the three groups ($P > 0.05$).

Table 2 depicts the results from the comparison of ONH characteristics in myopic groups, including structural parameters, optic disc tilt and rotation, focal LC defects, PPA, and MvD. The optic disc, RIM, β-PPA area, presence and area of γ-PPA, BMOD and BL increased with the increase of AL ($P \leq 0.001$). Group 1 showed more tilted disc ($P = 0.012$) than groups 2 and 3. In contrast, group 3 had a larger cup area ($P = 0.022$), more focal LC defect, and total, as well as juxtapapillary, MvD ($P \leq 0.001$) than those of groups 1 and 2. In addition, group 3 had a larger ratio of optic disc tilt than that of group 1 ($P = 0.011$).

Table 3 shows the relationships among the ONH parameters, SE, and AL. We adopted SE and AL as the explanatory variables in the different regression models. According to the univariate and multivariate analyses, SE significantly correlated with the optic disc area ($\beta = 0.710$; $P = 0.003$), rim area ($\beta = -0.630$; $P = 0.010$), β-PPA area ($\beta = 0.268$; $P < 0.001$), cup volume ($\beta = -0.265$; $P = 0.019$), γ-PPA area ($\beta = 0.219$; $P = 0.007$), focal LC defect ($\beta = 0.217$; $P < 0.001$), and presence of γ-PPA ($\beta = 0.154$; $P = 0.004$). Moreover, the BMOD ($\beta = 0.269$; $P = 0.009$), presence of γ-PPA

Table 1. Baseline Data for Myopic Groups

	Group 1	Group 2	Group3	*P* Value
Number	105	98	118	
Age (y), range	28.725 $\pm$ 5.868	29.020 $\pm$ 6.784	27.640 $\pm$ 6.079	0.238
Sex				<0.05
Male	25	36	48	
Female	80	62	70	
SE (D), range	3.194 $\pm$ 1.940	4.540 $\pm$ 1.635	7.296 $\pm$ 2.253	<0.001
AL (mm), range	24.218 $\pm$ 0.570	25.506 $\pm$ 0.294	27.036 $\pm$ 0.914	<0.001
IOP, range	14.249 $\pm$ 2.521	13.933 $\pm$ 2.717	14.170 $\pm$ 2.788	0.684
CCT, range	526.786 $\pm$ 35.720	535.260 $\pm$ 26.665	534.525 $\pm$ 31.834	0.106

CCT, central corneal thickness.

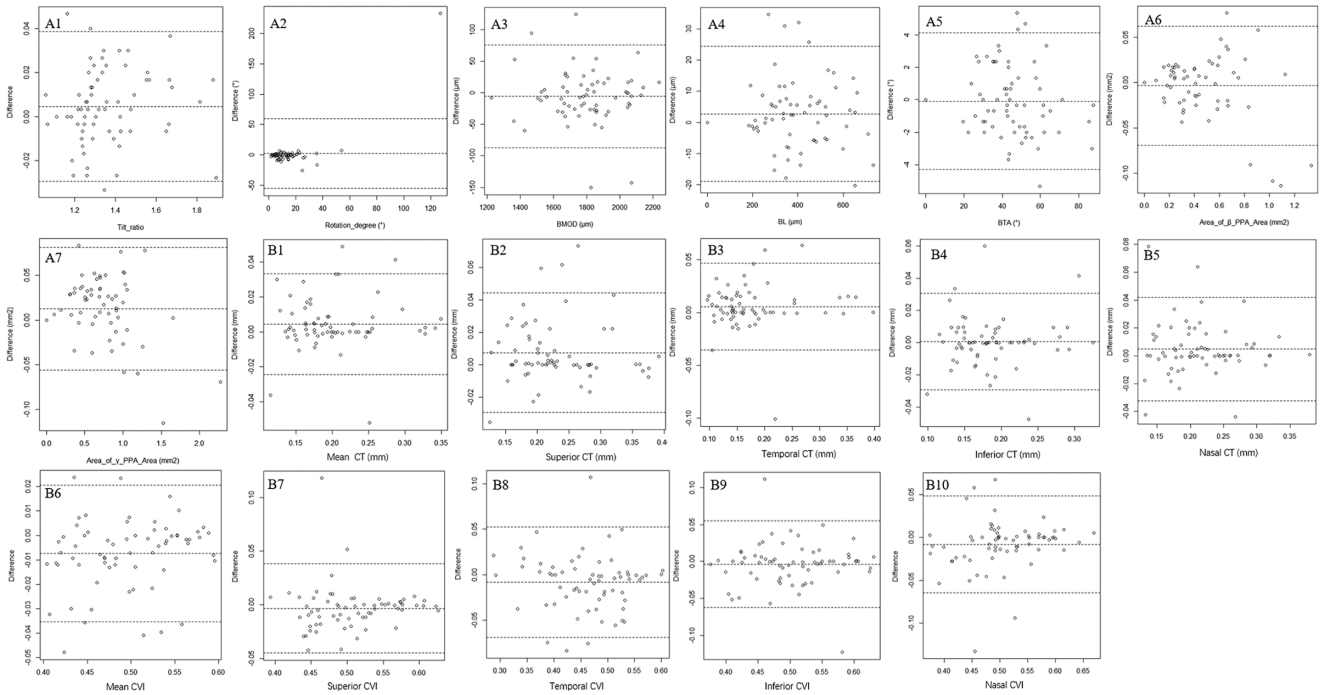

Figure 3. Reproducibility differences in the measurement of ONH and peripapillary parameters. Structural Parameters: A1–A7; Microvasculature Parameters: B1–B10.

Table 2. Comparison of ONH Characteristics in Three Myopic Groups

ONH Parameters	Group1	Group2	Group3	*P* Value
Mean C/D	0.47 ± 0.16	0.45 ± 0.16	0.45 ± 0.15	0.702
Cup area (mm^2)	0.60 ± 0.43	0.63 ± 0.46*	0.80 ± 0.73†	<0.05
Cup volume (mm^3)	0.54 ± 0.56	0.56 ± 0.59	0.58 ± 0.55	0.885
Optic disc area (mm^2)	2.32 ± 0.42‡	2.61 ± 0.47*	3.21 ± 1.48†	<0.001
RIM area (mm^2)	1.72 ± 0.30‡	1.99 ± 0.35*	2.41 ± 1.02†	<0.001
Vertical C/D	0.41 ± 0.15	0.40 ± 0.19	0.40 ± 0.14	0.786
Optic disc tilt				<0.05
Tilted disc	50‡	65	77†	
Disc without tilt	54‡	36	38†	
Tilt ratio	1.35 ± 0.18	1.39 ± 0.20	1.44 ± 0.23†	<0.05
Optic disc rotation				
Superior/inferior	44/58	53/44	62/52	0.169
Significant/insignificant	21/84	21/77	25/91	0.953
Rotation degree	9.17° ± 7.43°	10.78° ± 9.10°	11.57° ± 11.11°	0.169
ONH Unchange/change, if unchange, below (%)				
BMOD (μm)	1640.69 ± 198.04‡	1818.41 ± 250.12*	2056.52 ± 468.59†	<0.001
BL (μm)	277.84 ± 176.64‡	394.22 ± 196.49*	596.16 ± 318.26†	<0.001
BTA	44.15° ± 26.66°	43.16° ± 18.25°	39.91° ± 16.20°	0.293
Focal LC defect presence/absence	83/22	73/25*	65/53†	<0.001
β-PPA Area				
Presence/absence	90/15	88/9	105/13	0.524
Area of β-PPA(mm^2)	0.30 ± 0.24‡	0.45 ± 0.30*	0.59 ± 0.49†	<0.001
γ-PPA Area				
Presence/absence	76/29‡	91/6*	116/2†	<0.001
Area of γ-PPA Area(mm^2)	0.39 ± 0.30‡	0.62 ± 0.28	1.05 ± 1.07†	<0.001
MvD				
Presence/absence, no(%)	7/98	16/82*	50/68†	<0.001
Nonjuxtapapillary/juxtapapillary	5/2	10/5*	40/9†	<0.001

BTA, border tissue angle.
*Significant differences between group 2 and group 3.
†Significant differences between group 1 and group 3.
‡Significant differences between group 1 and group 2.

Investigative Ophthalmology & Visual Science

Table 3. Linear Regression Analysis To Determine the Correlations Between ONH Parameters and SE and AL

	Spherical Equivalent								Axial Length							
	Univariate Analysis				Multivariate Analysis				Univariate Analysis				Multivariate Analysis			
ONH Parameter	**B**	**β**	**95%CI**	**P Value**	**B**	**β**	**95%CI**	**P Value**	**B**	**β**	**95%CI**	**P Value**	**B**	**β**	**95%CI**	**P Value**
Mean C/D	−2.495	−0.154	−4.327, −0.664	0.008	−3.693	−0.226	−7.853, 0.468	0.083	−0.021	−0.002	−0.969, 0.928	0.966				
Cup area	0.332	0.074	−0.180, 0.845	0.205					0.455	0.198	0.197, 0.713	0.001	−2.084	−0.920	−23.719, 19.551	0.850
Cup volume	−0.522	−0.116	−1.032, −0.012	0.046	−1.188	−0.265	−2.178, −0.199	0.019	0.076	0.033	−0.186, 0.339	0.570				
Optic disc area	0.914	0.364	0.647, 1.180	<0.001	1.797	0.710	0.615, 2.979	0.003	0.588	0.458	0.457, 0.718	<0.001	2.058	1.618	−19.605, 23.722	0.852
RIM area	1.621	0.457	1.260, 1.981	<0.001	−2.250	−0.630	−3.951, −0.550	0.010	0.892	0.492	0.711, 1.073	<0.001	−1.768	−0.986	−23.422, 19.886	0.873
Vertical C/D	−2.418	−0.153	−4.204, −0.632	<0.01	−0.390	−0.025	−3.669, 2.888	0.816	0.096	0.012	−0.829, 1.021	0.839				
Optic disc tilt																
Tilted disc/disc without tilt	0.979	0.184	0.400, 1.558	0.001	−0.221	−0.043	−0.907, 0.464	0.528	0.378	0.141	0.085, 0.671	0.012	0.011	0.004	−0.340, 0.362	0.950
Tilt ratio	2.522	0.198	1.139, 3.906	<0.001	−0.345	−0.027	−2.326, 1.636	0.733	0.87	0.136	0.168, 1.572	0.016	−0.032	−0.005	−1.021, 0.957	0.949
Optic disc rotation																
Superior/inferior	0.443	0.084	−0.139, 1.026	0.137					0.257	0.097	−0.035, 0.549	0.086				
Significant/insignificant	−0.378	−0.059	−1.084, 0.328	0.294					0.17	0.052	−0.191, 0.530	0.357				
Rotation degree (°)	0.002	0.008	−0.029, 0.033	0.885					0.022	0.155	0.006, 0.037	0.006	0.006	0.041	−0.007, 0.018	0.374
ONH change																
BMOD (μm)	0.004	0.511	0.003, 0.004	<0.001	0	0.029	−0.001, 0.002	0.778	0.002	0.628	0.002, 0.003	<0.001	0.001	0.269	0.000, 0.002	0.009
BL (μm)	0.005	0.570	0.005, 0.006	<0.001	0.002	0.183	−0.000, 0.004	0.053	0.003	0.583	0.002, 0.003	<0.001	0.001	0.103	−0.000, 0.002	0.27
BTA (°)	−0.003	−0.463	−0.072, −0.047	<0.001	−0.014	−0.111	−0.032, 0.004	0.119	−0.029	−0.453	−0.035, −0.023	<0.001	−0.001	−0.014	−0.010, 0.008	0.843
Focal LC defect	2.053	0.361	1.472, 2.635	<0.001	1.194	0.217	0.689, 1.700	<0.001	0.844	0.29	0.538, 1.150	<0.001	0.364	0.132	0.109, 0.619	0.006
β-PPA Area																
Presence/absence	0.490	0.059	−0.414, 1.395	0.289					0.101	0.024	−0.363, 0.565	0.669				
Area of β-PPA (mm^2)	2.558	0.373	1.858, 3.258	<0.001	1.793	0.268	0.981, 2.604	<0.001	1.238	0.352	0.876, 1.600	<0.001	0.306	0.091	−0.102, 0.713	0.143
γ-PPA Area																
Presence/absence	2.966	0.360	2.120, 3.811	<0.001	1.230	0.154	0.395, 2.066	<0.001	1.577	0.373	1.147, 2.008	<0.001	0.644	0.161	0.222, 1.065	0.003
Area of γ-PPA (mm^2)	1.855	0.520	1.520, 2.190	<0.001	1.008	0.219	0.280, 1.736	<0.001	1	0.548	0.832, 1.168	<0.001	0.003	0.001	−0.354, 0.361	0.985
MvD																
Presence/absence	1.991	0.317	1.337, 2.645	<0.001	−0.125	−0.020	−1.859, 1.609	0.888	1.157	0.359	0.827, 1.486	<0.001	0.758	0.243	−0.122, 1.638	0.092
Nonjuxtapapillary/juxtapapillary	1.134	0.328	0.776, 1.492	<0.001	0.090	0.026	−0.849, 1.029	0.851	0.619	0.35	0.437, 0.801	<0.001	−0.226	−0.131	−0.701, 0.249	0.351

BTA, border tissue angle.

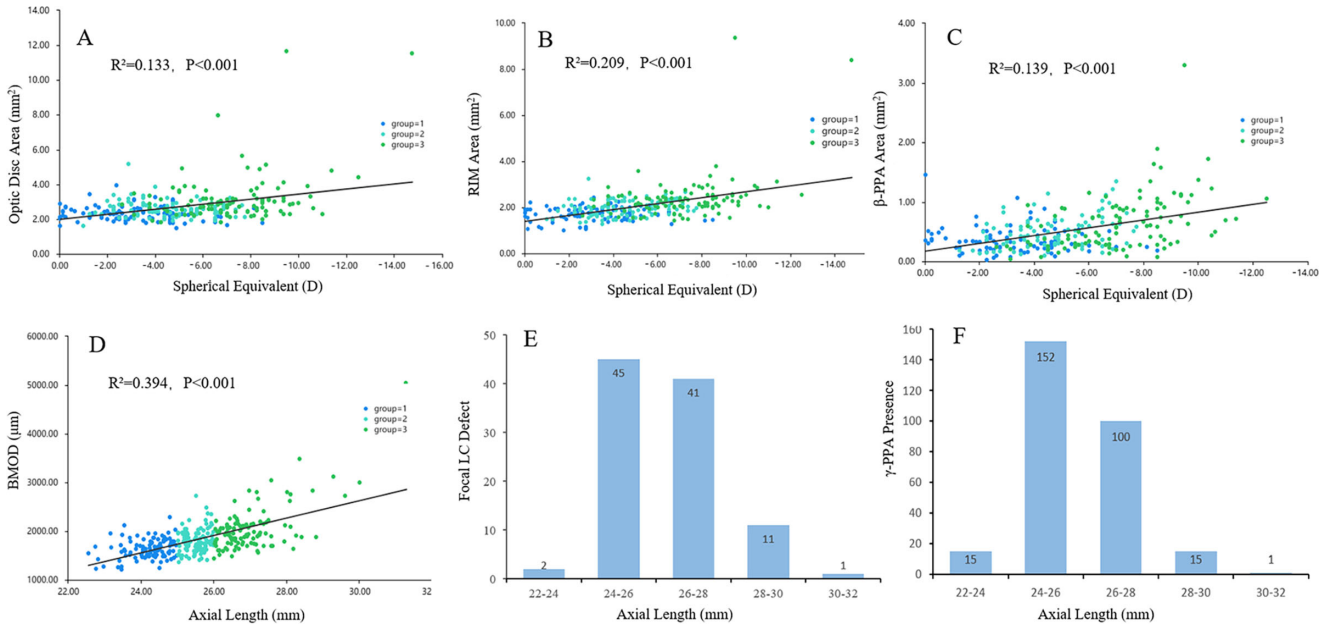

Figure 4. Scatterplots **(A–D)** showing the relationships between the spherical equivalent, axial length, and the top three parameters of standardized coefficient value in Table 3. Histogram **(E, F)** showing the distribution of the focal lamina cribrosa defect and the γ-PPA presence in myopic eyes with different axial lengths.

(β = 0.161; P = 0.003), and focal LC defects (β = 0.132; P = 0.006) were significant predictors of AL (Fig. 4).

As shown in Table 4, the mean, superior and temporal CT, central mean, temporal, pericentral mean, inferior and nasal RPC VD, and temporal CVI decreased with the increase of AL (P < 0.001). In contrast, the mean and temporal RNFL thickness increased (P < 0.001). Group 3 demonstrated a lower central superior, inferior and nasal, pericentral superior and temporal RPC VD than those observed with groups 1 and 2 ($P \leq$ 0.001). Group 1 had a larger inferior and nasal CT value, mean, superior, inferior, and nasal CVI than those observed from groups 2 and 3 (P < 0.001). According to the univariate and multivariate analyses, SE was significantly correlated with mean and temporal RNFL thickness (P < 0.001); mean, superior, temporal, and inferior CT (P < 0.001, P = 0.013, P < 0.001, and P = 0.006, respectively); central mean and temporal, pericentral mean, temporal (P < 0.001), and nasal RPC VD (P = 0.041); and mean and temporal CVI (P <0.001). The AL was associated with the mean and temporal RNFL thickness (P <0.001); mean, temporal, and inferior CT (P < 0.001, P < 0.001, and P = 0.028, respectively); central mean; temporal and nasal and pericentral mean; temporal RPC VD (P < 0.01); inferior RPC VD (P = 0.032); and mean, temporal (P < 0.001), and nasal ONH CVIs (P = 0.013, Fig. 5).

Discussion

Using SS-OCT and OCTA, we characterized the structural and microvasculature changes in the ONH according to the AL elongation. Myopic eyes were demonstrated to have larger optic disc and RIM area, tilted disc, ONH change, β- and γ-PPA area, mean and temporal RNFL, and MvD, but smaller mean and regional CT, RPC VD, and CVI. This finding could be partially supported by the histologic results stating that during axial elongation, disproportionate growth was found between regions and layers of the retina, choroid, and sclera.[25]

SS-OCT enables a fast scan rate and uses a light source with longer tunable wavelengths than SD-OCT.[13] Previous studies[9,11,26–29] have used SD-OCT to investigate the ONH parameters including optic disc tilt, rotation, BMOD, BL, BT angle, PPA, LC defect, RNFL, RPC and CT, which were also included in the current study. However, SS-OCT would be able to reduce motion artifact, and permits high-speed, high-resolution imaging and a better visualization of both shallow and deep ONH structures and choroidal microvasculature. In addition, to correct ocular magnification on the measurements, the scan size was adjusted because of different ALs among the eyes.[30] Therefore an SS-OCT instrument with the algorithm enabled accurate analysis of the ONH.

In this study, we demonstrated significant ONH structural variations in myopia. Histological studies have reported that the ONH comprises three layers, with the BMO and the opening in the choroid as its inner and middle layers, respectively, and the opening in the peripapillary scleral flange as the outer layer.[25] Our study found that BL and BMOD increased significantly with myopia. These observations were partly consistent with a previous longitudinal study.[9] However, they reported that the BMOD remained relatively stable during progression, most probably owing to the AL discrepancy, 24.80 mm in their study, and 25.65 mm in the current study. With axial elongation, Bruch's membrane generated in the retro-equatorial region leads to global disproportionate enlargement, which is more like a tube than like a sphere.[5] Kim et al.[31] reported that as the eyeball grows axially, the posterior pole elongates globally and also in a localized manner. During this process, the optic disc is pulled towards the deepest point of the elongated eyeball, resulting in a change in the optic disc.[31] In our study, myopic eyes with AL shorter than 25 mm had a larger degree of optic disc tilt than in the eyes with AL longer than 26 mm. In addition, the percentage of inferior optic disc rotation increased with myopia. Previous studies[11,32,33] reported that the inferior sclera expands more in highly myopic eyes.

Investigative Ophthalmology & Visual Science

Table 4. Comparison of Peripapillary RNFL, Choroidal Thickness, RPC Vessel Density, and CVIs and Linear Regression Between the ONH Parameters and SE and AL in Three Myopic Groups

					Spherical Equivalent				Axial Length			
Parameters	**Group1**	**Group2**	**Group3**	***P* Value**	**B**	**β**	**95% CI**	***P* Value**	**B**	**β**	**95% CI**	***P* Value**
RNFL thickness (μm)												
Mean	105.85 ± 12.83*	112.37 ± 11.45†	119.28 ± 17.40‡	<0.001	0.061	0.355	0.043, 0.079	<0.001	0.038	0.437	0.030, 0.047	<0.001
Superior	123.54 ± 26.41	129.27 ± 30.31	128.35 ± 34.63	0.355								
Temporal	67.70 ± 9.61*	77.65 ± 13.99†	97.75 ± 30.36‡	<0.001	0.06	0.556	0.051, 0.070	<0.001	0.033	0.588	0.028, 0.038	<0.001
Inferior	144.74 ± 29.38	138.33 ± 27.41	136.05 ± 36.26	0.11	−0.008	−0.093	−0.016, 0.000	0.059	−0.003	−0.062	−0.006, 0.001	0.170
Nasal	60.70 ± 10.93	59.65 ± 11.56	58.12 ± 13.98	0.289	−0.007	−0.032	−0.027, 0.014	0.517				
Choroidal thickness (μm)												
Mean	0.23 ± 0.06*	0.19 ± 0.05†	0.17 ± 0.04‡	<0.001	−18.486	−0.408	−23.079, −13.894	<0.001	−9.836	−0.423	−12.174, −7.498	<0.001
Superior	0.25 ± 0.07*	0.21 ± 0.05†	0.20 ± 0.05‡	<0.001	10.929	0.268	2.325, 19.533	0.013	3.055	0.146	−1.368, 7.478	0.177
Temporal	0.21 ± 0.07*	0.17 ± 0.06†	0.14 ± 0.05‡	<0.001	−29.385	−0.806	−37.068, −21.702	<0.001	−13.963	−0.747	−17.913, −10.014	<0.001
Inferior	0.21 ± 0.06*	0.17 ± 0.05	0.16 ± 0.04‡	<0.001	13.581	0.286	3.951, 23.211	0.006	5.587	0.229	0.636, 10.537	0.028
Nasal	0.24 ± 0.06*	0.20 ± 0.05	0.20 ± 0.05‡	<0.001	−8.086	−0.185	−16.804, 0.632	0.070	−1.812	−0.081	−6.293, 2.669	0.429
RPC Vessel Density												
Central mean	10.95 ± 3.07*	9.90 ± 2.82†	7.00 ± 3.11‡	<0.001	−0.390	−0.510	−0.462, −0.317	<0.001	−0.221	−0.566	−0.257, −0.186	<0.001
Central superior	6.66 ± 3.81	6.25 ± 3.71†	4.77 ± 3.67‡	<0.001	0.012	0.018	−0.052, 0.077	0.708	0.022	0.062	−0.006, 0.050	0.125
Central temporal	12.50 ± 6.37*	9.12 ± 6.58†	4.77 ± 4.37‡	<0.001	−0.123	−0.308	−0.165, −0.081	<0.001	−0.056	−0.275	−0.075, −0.038	<0.001
Central inferior	6.09 ± 2.85	6.04 ± 2.70†	3.88 ± 2.61‡	<0.001	−0.043	−0.047	−0.138, 0.052	0.378	0.003	0.007	−0.038, 0.044	0.886
Central nasal	18.54 ± 4.98	18.19 ± 5.28†	14.57 ± 6.18‡	<0.001	−0.019	−0.041	−0.064, 0.027	0.422	−0.028	−0.123	−0.048, −0.009	0.005
Pericentral mean	30.43 ± 2.44*	28.76 ± 3.07†	22.74 ± 5.74‡	<0.001	−0.307	−0.619	−0.350, −0.264	<0.001	−0.181	−0.713	−0.200, −0.161	<0.001
Pericentral superior	29.10 ± 3.12	27.86 ± 3.51†	22.32 ± 6.14‡	<0.001	−0.026	−0.053	−0.090, 0.039	0.436	−0.015	−0.061	−0.043, 0.013	0.294
Pericentral temporal	36.56 ± 3.56	35.25 ± 4.40†	24.84 ± 9.49‡	<0.001	−0.113	−0.363	−0.152, −0.074	<0.001	−0.072	−0.451	−0.089, −0.055	<0.001
Pericentral inferior	28.89 ± 3.55*	27.23 ± 3.49†	21.85 ± 5.48‡	<0.001	−0.007	−0.015	−0.069, 0.054	0.814	−0.03	−0.116	−0.056, −0.003	0.032
Pericentral nasal	27.18 ± 6.31*	24.71 ± 6.80†	21.97 ± 6.53‡	<0.001	−0.041	−0.107	−0.081, −0.002	0.041	−0.006	−0.029	−0.023, 0.012	0.519
ONH CVI												
Mean	0.52 ± 0.05*	0.49 ± 0.05	0.48 ± 0.05‡	<0.001	−12.86	−0.29	−17.574, −8.145	<0.001	−6.881	−0.302	−9.290, −4.473	<0.001
Superior	0.53 ± 0.06*	0.50 ± 0.06	0.50 ± 0.06‡	<0.001	2.806	0.07	−3.510, 9.122	0.385	1.567	0.076	−1.647, 4.782	0.340
Temporal	0.49 ± 0.06*	0.45 ± 0.07†	0.43 ± 0.09‡	<0.001	−10.201	−0.323	−14.864, −5.539	<0.001	−5.185	−0.32	−7.558, −2.812	<0.001
Inferior	0.52 ± 0.07*	0.49 ± 0.06	0.48 ± 0.06‡	<0.001	−0.945	−0.025	−6.536, 4.646	0.741	1.27	0.066	−1.575, 4.116	0.382
Nasal	0.54 ± 0.06*	0.50 ± 0.07	0.50 ± 0.06‡	<0.001	−3.293	−0.087	−9.372, 2.787	0.289	−3.922	−0.201	−7.016, −0.828	0.013

*Significant differences between groups 1 and 2.
†Significant difference between groups 2 and 3.
‡Significant difference between groups 1 and 3.

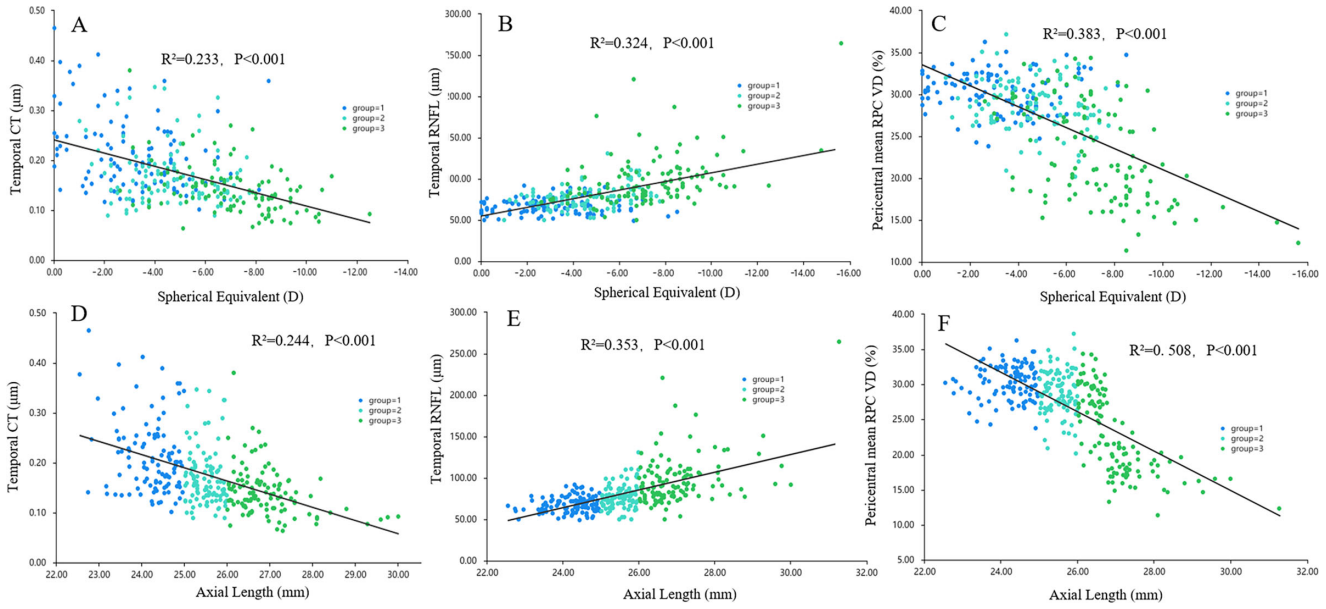

Figure 5. Scatterplots showing the relationships between the spherical equivalent, axial length, and the top three parameters of standardized coefficient values in Table 4. Temporal CT **(A, D)**; Temporal RNFL **(B, E)**; Pericentral mean RPC VD **(C, F)**.

The sclera in the lower half of the eye is the area where the embryonic ocular fissure closes, leading to a weaker structure. We found that the mean and temporal RNFL thickness increased in myopia, which was consistent with a recent study.[34] The reason might be the redistribution of parapapillary nerve fibers as the eye grows in length.[20] However, some researchers found that RNFL thickness was negatively correlated or had no relationship with AL using OCT.[35,36] The configuration of the myopic optic disc still remains controversial.

Meanwhile, we found a greater γ-PPA in early myopia, whereas the presence of β-PPA remained stable during the increase of AL, thus indicating the significance of early monitoring of γ-PPA. Both the area of β-PPA and γ-PPA increased with myopia. However, the pathogenesis of PPA remains controversial. Kim et al.[37] indicated that the PPA with intact BM may be an age-related atrophic change, whereas PPA lacking BM may result from the scleral stretching. Lee et al.[38] suggested that with axial elongation, the attachment is weaker between the inner retinal structure and outer walls (LC and sclera) than between the RPE and BM, the BM may be stretched, and the most prominent change occurs in the γ-zone. Furthermore, if the growth of the outer wall is too large to be compensated by shifting, the RPE might slide, especially when the attachment between the RPE and BM is not sufficiently strong, and ocular growth might lead to the enlargement of β-PPA. Our results are similar to the hypothesis proposed by Lee et al.[38] In addition, previous studies[11,25] have reported that monitoring optic disc torsion and β-PPA is a hot research topic involving high myopia and glaucoma.

Using the OCTA algorithm, combined with OCT B-scan images, we found dysfunction of the microvasculature in the RPC layer and the whole choroid layer in myopia. Our results showed that patients with myopia, especially high myopia, had significantly decreased RPC VD in either the foveal or parafoveal areas. The RPC blood flow density may change with the disproportionate growth of the eyeball. Furthermore, the changes in the flow density around the optic papilla are reported to precede those in the macula.[34] In addition, monitoring RPC blood flow is of great significance for the early diagnosis of patients with high myopia or glaucoma. Limited information is available on the peripapillary CVI in myopic eyes. This study showed that temporal CVI gradually decreased with the increase of myopia, and the nasal, superior, and inferior CVI decreased in group 1 compared to groups 2 and 3, but did not change significantly in group 3, suggesting that temporal CVI was more sensitive in myopic choroidal blood flow lesions.

In our study, MvD was found in 73 eyes (22.7%) and was similar to one previous study (19.8%),[26] which also investigated MvD in healthy myopic eyes. The frequency of MvD in patients with high myopia increased significantly, and most of the regions occurred in the γ region. This finding may be related to the mutual movement of the BM and scleral limbus tissue, thus suggesting deep vascular insufficiency. Previous studies have shown that MvD is closely associated with early parafoveal blind spots, suggesting it to be a vascular risk factor for glaucomatous optic neuropathy.[7] However, we speculated that the MvD in myopic eyes should have different pathogeneses from that in glaucomatous eyes based on the characteristic features. The previously reported MvD in glaucoma was considered a dropout of microvessels within the scleral flange.[39] And the MvD in myopia was associated with misalignment of the BM-RPE complex. SS-OCT enables a faster scan rate and would provide more accurate information of deep ONH structures and choroidal microvasculature, which adds to our understanding of MvD.

Linear regression analysis showed that BMOD, focal LC defects, and γ-PPA levels were positively correlated with AL. As the AL increases, we speculate that the BM stretches and shifts, and then γ-PPA occurs. Previous studies have suggested that the LC is deformed in myopia and also affects the axonal injuries in glaucoma.[40] Interestingly, β-PPA was not associated with AL but was positively associated with SE, thus indicating that the mechanism of β-PPA may not be related to the RPE sliding caused by axial extension.[41] The

CT and RNFL thickness in the temporal direction and paracentral RPC VD were the most important factors related to both the SE and AL, suggesting that the temporal quadrant and paracentric blood flow are more susceptible to damage.

Our study had some limitations. First, it was cross-sectional; therefore changes in the optic disc and various other parameters could not be documented. Longitudinal studies may be useful for overcoming this shortcoming. Second, some ONH parameters on OCT images were evaluated on the basis of subjective measurements, which may have led to certain measurement errors. However, we used Bland-Altman and kappa (κ) analyses and confirmed stable repeatability. Third, we only included healthy subjects without glaucoma. Thus it would be difficult to explain the association between myopia and glaucoma using the findings in the current study. However, according to previous studies, we speculated that the mechanisms that lead to visual field defects or RPC VD in myopia may be different from myopia with glaucoma.[42] Investigating the ONH changes related to myopia would provide basic information for glaucoma patients with myopia. Furthermore, it would be difficult to determine whether the reduced RPC, MvD and LC defects were caused by axial stretching or glaucoma lesions, if we included patients with both myopia and glaucoma.

In conclusion, we demonstrated the structural and microvasculature variations of the ONH that were associated with different AL using SS-OCT. Myopic ONH changes may be associated with the disproportionate growth of the retina, choroid, and sclera around the optic disc during axial elongation. These changes may provide an important clue to the mechanism of myopia and help to differentiate myopia from glaucoma. SS-OCT with image analysis may be useful in detecting ONH changes during myopia.

Acknowledgments

Supported by research grants from the National Natural Science Foundation of China (Grant No. 81900910), Basic Scientific Research Project of Wenzhou (Y20210194).

Disclosure: **D. Cheng,** None; **K. Ruan,** None; **M. Wu,** None; **Y. Qiao,** None; **W. Gao,** None; **H. Lian,** None; **M. Shen,** None; **F. Bao,** None; **Y. Yang,** None; **J. Zhu,** None; **H. Huang,** None; **X. Meng,** None; **L. Shen,** None; **Y. Ye,** None

References

1. Morgan IG, Ohno-Matsui K, Saw S-M. Myopia. *Lancet*. 2012;379(9827):1739–1748.
2. Li S-M, Wei S, Atchison DA, et al. Annual incidences and progressions of myopia and high myopia in Chinese schoolchildren based on a 5-year cohort study. *Invest Ophthalmol Vis Sci*. 2022;63:8.
3. Zhou X, Pardue MT, Iuvone PM, Qu J. Dopamine signaling and myopia development: What are the key challenges. *Prog Retin Eye Res*. 2017;61:60–71.
4. Jonas JB, Wang YX, Dong L, Guo Y, Panda-Jonas S. Advances in myopia research anatomical findings in highly myopic eyes. *Eye Vis (Lond)*. 2020;7:45.
5. Jonas JB, Ohno-Matsui K, Jiang WJ, Panda-Jonas S. Bruch membrane and the mechanism of myopization: A new theory. *Retina*. 2017;37:1428–1440.
6. Terasaki H, Yamashita T, Tanaka M, Nakao K, Sakamoto T. Relationship between funduscopic conus and optic disc factors associated with myopia in young healthy eyes. *Invest Ophthalmol Vis Sci*. 2020;61(2):40.
7. Kim G-N, Lee EJ, Kim T-W. Microstructure of Nonjuxtapapillary Microvasculature Dropout in Healthy Myopic Eyes. *Invest Ophthalmol Vis Sci*. 2020;61(2):36.
8. Park H-YL, Jeon SJ, Park CK. Features of the choroidal microvasculature in peripapillary atrophy are associated with visual field damage in myopic patients. *Am J Ophthalmol*. 2018;192:206–216.
9. Kim M, Choung HK, Lee KM, Oh S, Kim SH. Longitudinal changes of optic nerve head and peripapillary structure during childhood myopia progression on OCT: Boramae Myopia Cohort Study Report 1. *Ophthalmology*. 2018;125:1215–1223.
10. Suh MH, Zangwill LM, Manalastas PIC, et al. Deep retinal layer microvasculature dropout detected by the optical coherence tomography angiography in glaucoma. *Ophthalmology*. 2016;123:2509–2518.
11. Sung MS, Kang YS, Heo H, Park SW. Characteristics of optic disc rotation in myopic eyes. *Ophthalmology*. 2016;123:400–407.
12. Ding Z, Li P, Wang RR. Introduction to the Special Issue on Optical Coherence Tomography (OCT). 2021;14(01):2102001.
13. Lains I, Wang JC, Cui Y, et al. Retinal applications of swept source optical coherence tomography (OCT) and optical coherence tomography angiography (OCTA). *Prog Retin Eye Res*. Sep 2021;84:100951.
14. Barteselli G, Bartsch D-U, Weinreb RN, et al. Real-time full-depth visualization of posterior ocular structures: comparison between full-depth imaging spectral domain optical coherence tomography and swept-source optical coherence tomography. *Retina*. 2016;36:1153–1161.
15. Stanga PE, Tsamis E, Papayannis A, Stringa F, Cole T, Jalil A. Swept-source optical coherence tomography angio (Topcon Corp, Japan): technology review. *Dev Ophthalmol*. 2016;56:13–17.
16. Lopilly Park HY, Lee NY, Choi JA, Park CK. Measurement of scleral thickness using swept-source optical coherence tomography in patients with open-angle glaucoma and myopia. *Am J Ophthalmol*. 2014;157:876–884.
17. Asai T, Ikuno Y, Akiba M, Kikawa T, Usui S, Nishida K. Analysis of peripapillary geometric characters in high myopia using swept-source optical coherence tomography. *Invest Ophthalmol Vis Sci*. 2016;57:137–144.
18. Biswas S, Jhanji V, Leung CK. Prevalence of glaucoma in myopic corneal refractive surgery candidates in Hong Kong China. *J Refract Surg*. 2016;32:298–304.
19. Biswas S, Lin C, Leung CK. Evaluation of a myopic normative database for analysis of retinal nerve fiber layer thickness. *JAMA Ophthalmol*. 2016;134:1032–1039.
20. Choi YJ, Jeoung JW, Park KH, Kim DM. Glaucoma detection ability of ganglion cell-inner plexiform layer thickness by spectral-domain optical coherence tomography in high myopia. *Invest Ophthalmol Vis Sci*. 2013;54:2296–2304.
21. Tan CS, Ouyang Y, Ruiz H, Sadda SR. Diurnal variation of choroidal thickness in normal, healthy subjects measured by spectral domain optical coherence tomography. *Invest Ophthalmol Vis Sci*. 2012;53:261–266.
22. Han JC, Cho SH, Sohn DY, Kee C. The characteristics of lamina cribrosa defects in myopic eyes with and without open-angle glaucoma. *Invest Ophthalmol Vis Sci*. 2016;57:486–494.
23. Wu H, Zhang G, Shen M, et al. Assessment of choroidal vascularity and choriocapillaris blood perfusion in anisomyopic adults by SS-OCT/OCTA. *Invest Ophthalmol Vis Sci*. 2021;62(1):8.
24. Agrawal R, Gupta P, Tan K-A, Cheung CMG, Wong T-Y, Cheng C-Y. Choroidal vascularity index as a measure of vascular status of the choroid: measurements in healthy eyes from a population-based study. *Sci Rep*. 2016;6:21090.

25. Wang YX, Panda-Jonas S, Jonas JB. Optic nerve head anatomy in myopia and glaucoma, including parapapillary zones alpha, beta, gamma and delta: histology and clinical features. *Prog Retin Eye Res*. Jul 2021;83:100933.
26. Kim GN, Lee EJ, Kim TW. Microstructure of nonjuxtapapillary microvasculature dropout in healthy myopic eyes. *Invest Ophthalmol Vis Sci*. 2020;61:36.
27. Han JC, Cho SH, Sohn DY, Kee C. The characteristics of lamina cribrosa defects in myopic eyes with and without open-angle glaucoma. *Invest Ophthalmol Vis Sci*. 2016;57:486–494.
28. AttaAllah HR, Omar IAN, Abdelhalim AS. Evaluation of optic nerve head parameters and retinal nerve fiber layer thickness in axial myopia using SD OCT. *Ophthalmol Ther*. 2017;6:335–341.
29. Suh MH, Park JW, Khandelwal N, Agrawal R. Peripapillary choroidal vascularity index and microstructure of parapapillary atrophy. *Invest Ophthalmol Vis Sci*. 2019;60:3768–3775.
30. Dai Y, Xin C, Zhang Q, et al. Impact of ocular magnification on retinal and choriocapillaris blood flow quantification in myopia with swept-source optical coherence tomography angiography. *Quant Imaging Med Surg*. 2021;11:948–956.
31. Kim YC, Jung Y, Park H-YL, Park CK. The location of the deepest point of the eyeball determines the optic disc configuration. *Sci Rep*. 2017;7(1):5881.
32. Choi JA, Park H-YL, Shin H-Y, Park CK. Optic disc tilt direction determines the location of initial glaucomatous damage. *Invest Ophthalmol Vis Sci*. 2014;55:4991–4998.
33. Ohno-Matsui K, Akiba M, Modegi T, et al. Association between shape of sclera and myopic retinochoroidal lesions in patients with pathologic myopia. *Invest Ophthalmol Vis Sci*. 2012;53:6046–6061.
34. Lin T, Su L, Lin J, Qiu H. Study on the optic nerve fiber layer thickness and changes in blood flow in myopic children. *Int J Gen Med*. 2021;14:3287–3293.
35. Arranz-Marquez E, Lauzirika G, Teus MA, Katsanos A. Thinner retinal nerve fibre layer in healthy myopic eyes with thinner central corneal thickness. *Graefes Arch Clin Exp Ophthalmol*. 2020;258:2477–2481.
36. Al-Sheikh M, Phasukkijwatana N, Dolz-Marco R, et al. Quantitative OCT angiography of the retinal microvasculature and the choriocapillaris in myopic eyes. *Invest Ophthalmol Vis Sci*. 2017;58:2063–2069.
37. Kim M, Kim TW, Weinreb RN, Lee EJ. Differentiation of parapapillary atrophy using spectral-domain optical coherence tomography. *Ophthalmology*. 2013;120:1790–1797.
38. Lee KM, Choung HK, Kim M, Oh S, Kim SH. Change of beta-zone parapapillary atrophy during axial elongation: Boramae Myopia Cohort Study Report 3. *Invest Ophthalmol Vis Sci*. 2018;59:4020–4030.
39. Lee EJ, Kim JA, Kim TW, Kim H, Yang HK, Hwang JM. Glaucoma-like parapapillary choroidal microvasculature dropout in patients with compressive optic neuropathy. *Ophthalmology*. 2020;127:1652–1662.
40. Sawada Y, Araie M, Ishikawa M, Yoshitomi T. Multiple temporal lamina cribrosa defects in myopic eyes with glaucoma and their association with visual field defects. *Ophthalmology*. 2017;124:1600–1611.
41. Sullivan-Mee M, Patel NB, Pensyl D, Qualls C. Relationship between juxtapapillary choroidal volume and beta-zone parapapillary atrophy in eyes with and without primary open-angle glaucoma. *Am J Ophthalmol*. 2015;160:637–647.
42. Lanca C, Sun CH, Chong R, et al. Visual field defects and myopic macular degeneration in Singapore adults with high myopia [published online ahead of print April 22, 2021]. *Br J Ophthalmol*, doi:10.1136/bjophthalmol-2020-318674.